Enhancing Communication Resilience through Fluid Antenna Index Modulation

Yinglin Chen*, Hao Xu†, and Tongyang Xu‡

*6G Research Center, China Telecom Research Institute, Guangzhou, 510660, China
†Department of Electronic and Electrical Engineering, University College London, London, WC1E 7JE, United Kingdom
‡School of Engineering, Newcastle University, Newcastle upon Tyne, NE1 7RU, United Kingdom
Email: chenyl37@chinatelecom.cn, hao.xu@ucl.ac.uk, tongyang.xu@newcastle.ac.uk

***Abstract*—Advanced anti-eavesdropping techniques play a crucial role in ensuring the security and reliability of 6G communication systems. Index modulation (IM) has attracted attention due to its enhanced power efficiency achieved by the implicit index domain information, alongside explicit data symbol modulation. Given the distinct characteristics of bit transmission in IM, anti-eavesdropping methods specifically designed for novel IM schemes are required. This work proposes a secure fluid antenna index modulation (S-FAIM) framework to safeguard both index and data symbol transmissions against eavesdropping. Secure index transmission is achieved by randomizing the mapping between index bits and channel conditions, created by fluid antenna port positions, based on the channel state information of the legitimate link. Furthermore, data symbol transmission is protected by a combined configuration of non-orthogonal spectrally efficient frequency division multiplexing (SEFDM) waveforms and channel coding. In addition to constant error floors at 0.5 observed at the eavesdropper for both index and data symbol transmissions, the proposed framework enhances the reliability performance of the legitimate user. With a robust wavelet scattering neural network deployed for channel condition classification, data symbol transmission achieves error performance comparable to that of conventional non-IM SEFDM and orthogonal frequency division multiplexing (OFDM) systems. Moreover, additional index transmission, reliant on channel variations, demonstrates resilience against deep fades and exhibits improved error performance over data symbol transmission.**

***Index Terms*—Index modulation, OFDM, SEFDM, fluid antenna, physical layer security, eavesdropping, wavelet scattering.**

I. Introduction

In 6G communication systems, the importance of security grows alongside the envisioned ubiquitous connection. One of the significant challenges that secure wireless communication faces is eavesdropping due to its broadcast nature. While conventional upper-layer security methods contend with high computational complexity and overhead burden, physical layer security (PLS) techniques have gained research interests for their ability to overcome the above issues [1].

PLS techniques leverage wireless communication channel characteristics to safeguard the transmission against eavesdropping. By exploiting the reciprocity of the channel, the legitimate transmitter Alice and the legitimate receiver Bob can generate shared secret keys, which are used to encrypt and decrypt the transmitted data. This renders the eavesdropper Eve unable to decrypt the transmitted data, as Eve lacks access to the channel conditions of the legitimate link. These keys, derived from variations in the time, frequency, or spatial domains of the channel, offer an effective solution to key management problems [2], [3]. However, implementing such encryption methods entails additional processing at both the receiver and transmitter, and the decryption performance has a significant influence on the reliability of legitimate transmission.

Channel conditions serve not only as the foundation for developing PLS techniques but also find application in index modulation (IM). IM is a trending modulation scheme that transmits information bits through the indices of communication entities, in addition to conventional data symbol transmission. Depending on the altered communication entities, IM can be grouped to frequency-domain IM, time-domain IM, and spatial-domain IM [4], [5]. Conventional spatial-domain IM rely on multiple antennas. Spatial modulation (SM) [6] maps index bits into the activation pattern of transmit antennas. To simplify transmitter design, media-based modulation (MBM) [7], [8] was introduced, leveraging multiple RF mirrors—passive antenna elements with PIN diodes—positioned around a single transmit antenna. By manipulating the on/off state of RF mirrors, different radiation patterns are generated and then selected based on index bits. Recently in [9]–[11], with the integration of fluid antenna technologies, IM patterns were created by altering the positions of fluid antennas. This design results in a flexible and compact transmitter design without relying on fixed RF mirrors. In [11], fluid antenna index modulation (FAIM) was designed with orthogonal frequency division multiplexing (OFDM) waveforms. Moreover, to alleviate the computationally intensive task of traditional maximum-likelihood detection, a wavelet scattering neural network was employed for fast index pattern classification.

In addition to OFDM waveforms, non-orthogonal waveforms such as spectrally efficient frequency division multiplexing (SEFDM) have been incorporated into IM designs, with desirable error and power performance reported in [12]. However, research on the combination of SEFDM waveforms and fluid antenna-based IM is missing. Moreover, the information security issue of fluid antenna-based IM is unaddressed.

To address the aforementioned issues, a secure fluid antenna index modulation (S-FAIM) system is designed utilizing

SEFDM signal waveforms. This system leverages different channel conditions, created by adjusting a fluid antenna, as index patterns. At the receiver, a wavelet scattering neural network is employed for accurate index pattern identification. To our knowledge, this is the first use of non-orthogonal fluid antenna-based IM system. Recognizing the distinct nature of index and data symbol transmissions, we employ two PLS techniques to independently secure each transmission. For the index part, a fluid antenna port selection rule is randomized based on the information of legitimate channels, accessible exclusively to the legitimate user. Meanwhile, for the data symbol transmission, SEFDM waveforms are designed to confuse the eavesdropper with OFDM waveforms, thus disabling Eve from recovering the transmitted SEFDM data symbols. Furthermore, low-density parity-check (LDPC) coding is adopted in the data symbol transmission to mitigate the inter-carrier interference (ICI) impacts due to SEFDM modulation and enhance the reliability of legitimate transmission.

II. S-FAIM System Model

This section presents the system model for S-FAIM. As depicted in Fig. 2, the input data bits for each signalling interval is applied to LDPC coding before being mapped to M-ary data symbols. Subsequently, a data symbol vector $\mathbf{s} = [s_1, s_2, \cdots, s_{N_S}]^T$ is constructed, with each entry s_n belonging to the constellation alphabet $\mathcal{M}$. Here, N_S denotes the number of SEFDM subcarriers and $[\cdot]^T$ is the transpose operator. Following this, SEFDM modulation is performed by $\mathbf{x} = \mathbf{\Phi s}$, where $\mathbf{\Phi}$ represents the $N_S \times N_S$ carrier matrix given by the expression:

$$\mathbf{\Phi}_{k,n} = \left(1/\sqrt{N_S}\right) e^{j2\pi\alpha \frac{kn}{N_S}}, \tag{1}$$

with $\alpha \in (0, 1]$ denoting the bandwidth compression factor. It will be shown in the next section that the combined configuration of SEFDM waveforms and LDPC coding facilitates secure data symbol transmission. A cyclic prefix is taken from the end of the time-domain signal vector $\mathbf{x}$ and inserted to its beginning. After that, digital to analog conversion (DAC) is performed to convert the processed signal into radio waves for transmission.

On the other hand, index bits are embedded in the channel conditions experienced by the transmitted signal. A fluid antenna is equipped with software-controllable fluidic or non-fluidic materials (e.g., switchable pixels), capable of the reconfiguration of polarization, operating frequency, radiation patterns, and other relevant characteristics [13]. An illustrative example of a tube-like fluid antenna is shown in Fig. 2, where conductive fluid moves freely to different positions within the tube, referred to as ports, to generate desirable channel conditions. The channel condition associated with each port serves as an index pattern. For a fluid antenna with 2^L available ports, one port is selected for each signalling interval and its index conveys up to L index bits. To ensure the independence and distinguishability of spatial features radiated from each port, ports are positioned with sufficient spacing beyond half the wavelength.

The frequency-selective Rayleigh fading channel corresponding to the l-th port is represented as

$$\mathbf{h}_l = [h_{l,1}, h_{l,2}, \cdots, h_{l,V}]^T, \tag{2}$$

where $l = 1, 2, \cdots, 2^L$ and $h_{l,v}$ for $v = 1, 2, \cdots, V$ follows a complex Gaussian distribution with zero mean and variance $1/V$, denoted as $\mathcal{CN}(0, 1/V)$ and V is the number of paths. The mapping between input index bits and the activated port is randomized based on the channel state information (CSI) of the legitimate link, so that the index transmission is robust against eavesdropping. Details of the selection rule are provided in Section III.

Following its conversion back to digital form, the received signal is directly fed into a wavelet scattering neural network, as illustrated in Fig. 3. This multi-layer wavelet scattering framework is designed to extract stable features resilient to translations and deformations in input signals [14], [15]. When applied to S-FAIM signal classification in this paper, this multi-layer scattering network exhibits robustness, especially in scenarios where channels exhibit minor variations. Additionally, the primary focus of the wavelet scattering network is on extracting frequency-selective channel patterns, and therefore its complexity is lower than that of the traditional maximum-likelihood algorithm when considering high modulation formats and a lager number of subcarriers.

The architecture of the wavelet scattering neural network is provided as follows. As emphasized in [15], frequency averaging is essential to alleviate deformation instability. Given that frequency-domain averaging is analogous to time-domain averaging via a filter, the initial stage in wavelet scattering involves applying a time-average operation, formulated as $Ws_0 = x * \phi(t)$, where $\phi(t)$ denotes a lowpass filter characterized by the translation invariance time period.

The utilization of the lowpass filter $\phi(t)$ leads to the loss of information by filtering out high-frequency components. To recover these components, a set of wavelets is applied to the original input signal x through a series of wavelet modulus transforms, given by

$$Wm_0 = \begin{cases} |x * \psi_{1,1}(t)| \\ |x * \psi_{1,2}(t)| \\ \vdots \\ |x * \psi_{1,Q_1}(t)| \end{cases}, \tag{3}$$

where $\psi_{i,j}(t)$ denotes a wavelet at the i-th scattering layer with the j-th wavelet resolution. This array operation, defined in (3), illustrates the operations at the first scattering layer ($i = 1$). The parameter Q_1, determining the resolution of the wavelet transform, referred to as the number of wavelets per octave, dictates the number of wavelets at this scattering layer. Subsequently, the first-layer wavelet scattering coefficients, post averaging operations, are given by

$$Ws_1 = \begin{cases} |x * \psi_{1,1}(t)| * \phi(t) \\ |x * \psi_{1,2}(t)| * \phi(t) \\ \vdots \\ |x * \psi_{1,Q_1}(t)| * \phi(t) \end{cases}. \tag{4}$$

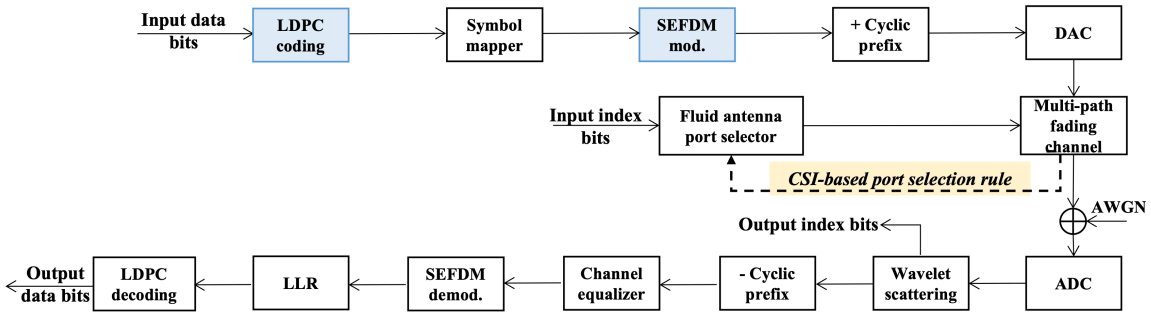

Fig. 1. Block diagram of the S-FAIM system where the channel condition created by selecting a fluid antenna port serves index transmission. Secure index transmission is enabled by the orange module and secure data symbol transmission is enabled by the blue modules. Details of security designs are provided in Section III.

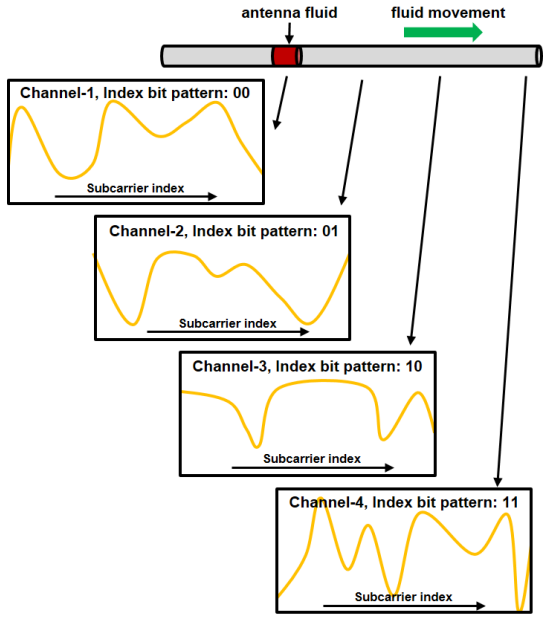

Fig. 2. S-FAIM system with a tube-like fluid antenna capable of generating four distinct channel conditions, corresponding to four 2-bit index patterns.

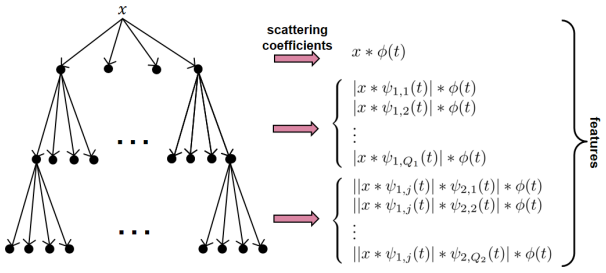

Fig. 3. Illustration of a wavelet scattering neural network.

Repeating the similar wavelet convolution and modulus averaging procedures, the second-layer wavelet scattering coefficients can be calculated as

$$Ws_2 = \begin{cases} ||x * \psi_{1,j}(t)| * \psi_{2,1}(t)| * \phi(t) \\ ||x * \psi_{1,j}(t)| * \psi_{2,2}(t)| * \phi(t) \\ \vdots \\ ||x * \psi_{1,j}(t)| * \psi_{2,Q_2}(t)| * \phi(t) \end{cases}. \tag{5}$$

As the second-layer wavelet convolves with all the wavelet modulus coefficients from the first layer, the number of operations increases at the second layer. In (5), the variable j ranges from 1 to Q_1. For each specific value of j, Q_2 wavelet convolutions are required. Typically, Q_2 is chosen to be smaller than Q_1 to obtain a sparse representation.

The number of wavelet scattering layers is contingent upon the specific application, with researchers in [15] suggesting that a two-layer scattering architecture is usually sufficient for many practical scenarios. Comprising wavelet convolution, modulus computation, and averaging operations, the wavelet scattering network offers a distinctive advantage: all filters are predetermined by wavelets, eliminating the necessity for learning from training data. This characteristic proves particularly advantageous for applications subject to limited training data availability. Furthermore, the efficiency of feature extraction is partially determined by the wavelet resolution parameter parameter Q. A higher Q value produces features with higher frequency resolution but at the expense of increased computational complexity. According to [15], the optimal value of Q typically lies between one and eight.

Based on the classification results reported by the wavelet scattering neural network, the estimated output index bits are determined by referencing the port selection rule. These classification results are also used for channel equalization after cyclic prefix removal. Subsequently, SEFDM demodulation is conducted by the following

$$\mathbf{y} = \mathbf{\Phi}^* \hat{\mathbf{H}}_l^* \mathbf{H}_l \mathbf{\Phi} \mathbf{s} + \mathbf{w} = \Lambda \mathbf{s} + \mathbf{w}, \tag{6}$$

where the matrix $\mathbf{H}_l$, constructed from $\mathbf{h}_l$, contains the CSI of the selected channel. $\hat{\mathbf{H}}_l^*$ corresponds to the complex conjugate of the channel matrix output by wavelet scattering. When the channel condition is accurately identified, i.e., $\mathbf{H}_l = \hat{\mathbf{H}}_l$, fading effects are mitigated. Otherwise, the non-one diagonal entries of the matrix $\Lambda = \mathbf{\Phi}^* \hat{\mathbf{H}}_l^* \mathbf{H}_l \mathbf{\Phi}$ characterise fading

TABLE I
AN EXAMPLE MAPPING TABLE FOR S-FAIM WITH CSI-BASED RANDOMIZED PORT SELECTION RULE.

Index bit pattern	*Selected fluid antenna port before / after randomization*	*Selected channel condition before / after randomization*
$[0,0]$	1 / 3	$\mathbf{H}_1$ / $\mathbf{H}_3$
$[0,1]$	2 / 1	$\mathbf{H}_2$ / $\mathbf{H}_1$
$[1,0]$	3 / 4	$\mathbf{H}_3$ / $\mathbf{H}_4$
$[1,1]$	4 / 2	$\mathbf{H}_4$ / $\mathbf{H}_2$

effects resulting from channel classification errors. In addition, additive white Gaussian noise (AWGN) samples are given by the vector $\mathbf{w}$ with the distribution of $\mathcal{CN}(0, N_0)$, and N_0 denotes the noise variance.

The log-likelihood ratio (LLR), defined as the logarithm of the probability ratio of a zero being transmitted versus an one being transmitted given a received signal, is computed based on the demodulated signal $\mathbf{y}$. Subsequently, the LLR outcomes are fed into the LDPC decoding block, which produces the final data bits transmitted through the legitimate link. A compact hardware design with low energy consumption is desired to implement wavelet scattering and LDPC decoding at the receiver.

III. Security Designs for Index and Data Symbol Transmissions

This section describes the detailed operations to guarantee secure bit transmission for the index and data parts of S-FAIM.

A. Secure Index Transmission

The security of index transmission relies upon the accessibility of the mapping rule, as the demodulation of index bits relies on its availability. It is commonly assumed that Eve does not have access to the mapping rule and therefore cannot recover index bits even if Eve successfully identifies the channel. To further enhance the secrecy of index transmission, a randomized port selection rule between index bits and the activated port of a fluid antenna is proposed. The rule is dependant on the CSI of the legitimate link from Alice to Bob (A2B link), rendering it inaccessible to Eve. In this paper, we use the channel gains of the SEFDM subcarriers for randomization. Table I provides an example look-up table for S-FAIM, in compared to FAIM with fixed mapping in [11]. With randomized mapping, the channel gains of the first S-FAIM subcarrier in four possible channels are in a descending order, given by $|\mathbf{H}_3(1,1)| > |\mathbf{H}_1(1,1)| > |\mathbf{H}_4(1,1)| > |\mathbf{H}_2(1,1)|$. Alternative CSI-based ordering methods can be applied, leading to randomized mapping strategies only known to the legitimate user. Results in the next section verify that Eve has to randomly estimate index bits and the resulting index bit error rate (BER) is at 0.5.

B. Secure Data Symbol Transmission

Secure data symbol transmission is proposed by exploiting the inherent difficulty of distinguishing between OFDM and SEFDM waveforms. SEFDM achieves bandwidth saving by reducing subcarrier spacing, given by

$$\text{BW}_S = \alpha N_S / T, \tag{7}$$

where N_S is the number of SEFDM subcarriers and T is the symbol period. Likewise, the bandwidth of an OFDM waveform with N_O subcarriers is given by

$$\text{BW}_O = N_O / T. \tag{8}$$

Based on (7) and (8), more SEFDM subcarriers than OFDM can be accommodated within the same spectrum occupancy. While Eve could identify a multi-carrier waveform by detecting the cyclic prefix, distinguishing between an OFDM and an SEFDM waveform is challenging as long as the signal bandwidth is kept the same. As exemplified in Fig. 4, the received SEFDM with $\alpha = 0.8$ and $N_S = 320$ and OFDM with $\alpha = 1$ and $N_O = 256$ exhibit identical channel responses. By configuring the bandwidth compression level and the subcarrier number of SEFDM waveforms following

$$N_O = \alpha N_S, \tag{9}$$

the resultant SEFDM waveforms show the same channel responses as that of OFDM. With this configuration, Alice transmits SEFDM waveforms with bandwidth compression levels known to Bob, who subsequently performs SEFDM demodulation following (6). However, for Eve, OFDM transmission is estimated and OFDM demodulation is performed using the OFDM carrier matrix $\mathbf{F}$, which is a specific form of $\mathbf{\Phi}$ when $\alpha = 1$ in (1). The demodulated signal at Eve is expressed as

$$\mathbf{y}_{eve} = \mathbf{F}^* \hat{\mathbf{H}}_z^* \mathbf{H}_z \mathbf{\Phi} \mathbf{s} + \mathbf{w}, \tag{10}$$

where $\hat{\mathbf{H}}_z^*$ and $\mathbf{H}_z$ belong to the set of possible wiretap links from Alice to Eve (A2E link), different to A2B link. Even if Eve correctly identifies the channel condition, the mismatch between the carrier matrices $\mathbf{F}^*$ and $\mathbf{\Phi}$ leads to poor demodulation performance.

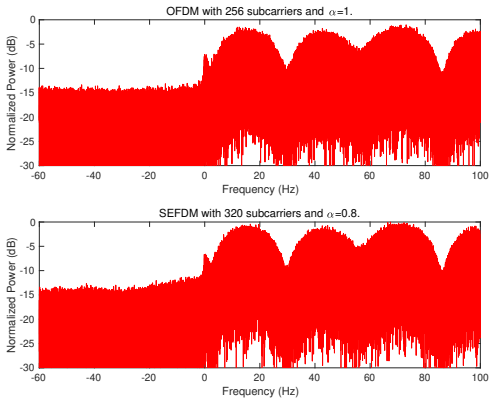

Fig. 4. Spectrum of the received S-FAIM signals with OFDM and SEFDM waveforms transmitted through the same frequency-selective fading channel.

Since the number of SEFDM subcarriers is higher than that of OFDM, SEFDM waveforms inherently convey a greater number of data bits compared to OFDM under the same modulation formats. To mitigate the ICI caused by the non-orthogonal SEFDM modulation and channel equalization errors due to incorrect index pattern classification, represented by the non-zero off-diagonal entries in the matrix Λ given in (6), LDPC coding is adopted for the data bit transmission, with the code rate $\mathcal{R} = \alpha$. In other words, the extra $(N_S - N_O)$ SEFDM subcarriers are allocated to carry parity-check bits, thus avoiding fluctuations in transmission rates. The LDPC coding procedure makes Eve more difficult to recover data bits, as Eve performs symbol demapping using hard decisions [16], [17]. Despite improved reliability and security, the computational complexity of coding imposes demands on the processing capabilities of Alice and Bob.

IV. Simulation Results and Discussions

This section presents the error performance of S-FAIM systems at Bob and Eve to verify the anti-eavesdropping capability of the proposed system. Moreover, the BER results of conventional non-IM fluid antenna systems with OFDM and SEFDM waveforms are provided to demonstrate the enhanced reliability performance of S-FAIM.

To investigate index patterns with $L = 2$ and $L = 3$ index bits, up to eight S-FAIM signal patterns corresponding to eight channel conditions are needed. We reuse a frequency-selective fading channel, given by $\mathbf{h}_1 = \left[0.8765, -0.2279, 0, 0, 0.1315, 0, 0, -0.4032e^{j\pi/2}\right]^T$ from [11], and generate the other seven channel patterns by introducing random normal distribution coefficients to $\mathbf{h}_1$. It is noted that $\mathbf{h}_1$ serves as a base channel model here, and various other channel models can be employed. To mimic OFDM waveforms with $N_O = 256$ subcarriers, this work considers two SEFDM waveforms, denoted as SEFDM-1 with $N_S = 284$ and $\alpha = 0.9$, and SEFDM-2 with $N_S = 320$ and $\alpha = 0.8$. 4QAM modulation is adopted for all waveforms. The LDPC code rates for systems with SEFDM-1 and SEFDM-2 waveforms are 0.9 and 0.8, respectively, with parity-check matrices from the DVB-S.2 standard. No coding is performed when operated with OFDM waveforms to achieve the same spectral efficiency. The received S-FAIM symbol comprises 512 samples, out of which 256 samples are truncated to ensure robustness against imperfect timing. The remaining 256 samples are sent into a two-layer wavelet scattering network, with $Q_1 = 8$ Morlet wavelet filters per octave in the first scattering layer to achieve high-frequency resolution and $Q_2 = 1$ Morlet wavelet filter in the second scattering layer for reduced computational complexity, consistent with the architecture in [11]. In addition to classification accuracy, the BER performance of index bits is provided by comparing the input and output index bits. Similarly, the data BER of S-FAIM is computed by comparing the data bits.

Since Bob is aware that SEFDM waveforms are used for data symbol transmission, SEFDM symbols are used for training. During the testing stage, another 1000 SEFDM testing symbols for each signal class are generated to model Bob's receiving performance. In Fig. 5, the accuracy of Bob's receiv-

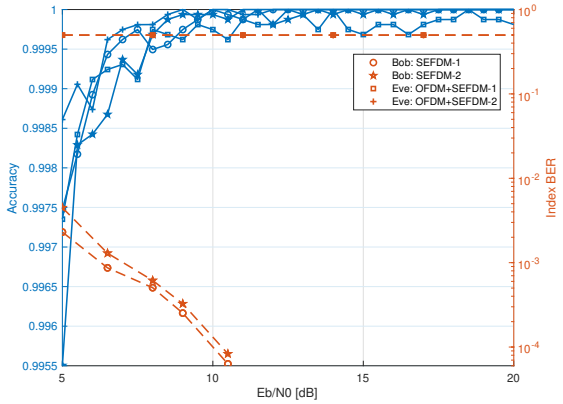

Fig. 5. Classification accuracy and index BER performance at Bob and Eve with 4-port S-FAIM when TSSC = 1.

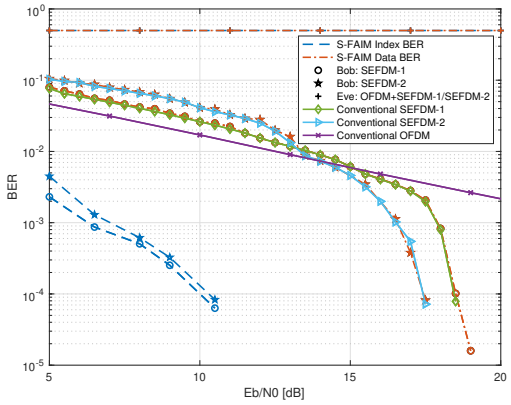

Fig. 6. BER performance at Bob and Eve with 4-port S-FAIM when TSSC = 1, compared with conventional non-IM OFDM and SEFDM systems.

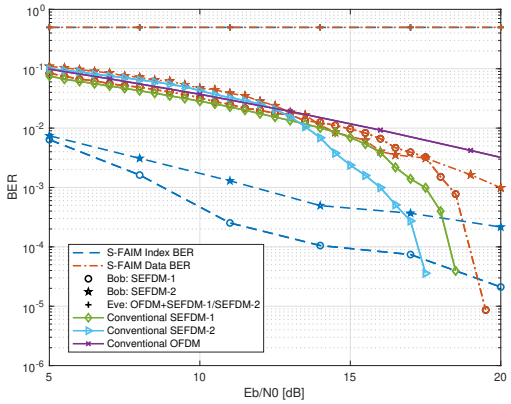

Fig. 7. BER performance at Bob and Eve with 8-port S-FAIM when TSSC = 2, compared with conventional non-IM OFDM and SEFDM systems.

ing with SEFDM-1 and SEFDM-2 waveforms reaches 1 with only one training symbol per signal class (TSSC), denoted as TSSC $= 1$. Eve is unaware of the transmission being SEFDM and consistently assumes OFDM transmission. Therefore, OFDM symbols are used for training, while SEFDM symbols are employed for testing to simulate Eve's performance. These configurations are labeled as OFDM+SEFDM-1/SEFDM-2, depending on the testing symbol setup. Although different waveforms are used for training and testing, the classification accuracy at Eve remains high, indicating the robustness of the proposed wavelet scattering network. Although Eve can accurately identify the channel condition, Eve cannot recover index bits as the mapping rule randomized by the CSI of A2B link is not accessible to her. Consequently, the index BER for Eve is constantly high at 0.5.

The data BER of the 4-port S-FAIM system at Bob and Eve is provided in Fig. 6. With the high index pattern classification accuracy reported in Fig. 5 and LDPC coding, the data BER aligns with that of conventional non-IM SEFDM systems with the same code rate, showing that the additional index transmission does not compromise data symbol transmission. Conversely, the conventional OFDM system of the same spectral efficiency with no LDPC coding exhibits a higher BER. Furthermore, the index part of S-FAIM with SEFDM-1 waveforms demonstrates a performance gain of 11 dB at the BER of 10^{-3} compared to its data part. This occurs because the data BER performance is susceptible to channel conditions while index transmission relying on channel variations is robust to deep fade effects. More importantly, this observation suggests the promising application of index transmission in severely jammed scenarios. For example, when Eve performs active jamming to disrupt the legitimate transmission, the index part is robust to attacks. On the other hand, due to erroneous demodulation and decoding processes, the data BER results at Eve with either SEFDM-1 or SEFDM-2 waveforms for testing fail with high error floors at 0.5.

When extending the index pattern to $L = 3$ bits, an additional training symbol indicated by TSSC $= 2$ is required to train a robust classifier for an 8-port S-FAIM system. In the low E_b/N_0 regime shown in Fig. 7, the index transmission of at Bob employing SEFDM-1 and SEFDM-2 waveforms surpasses their data counterparts. Due to incorrect index pattern classification, the data part of S-FAIM exhibits performance degradation compared to the conventional non-IM SEFDM signals, which can be addressed with an expanded training dataset. Nevertheless, a performance advantage of S-FAIM over non-IM OFDM systems is observed at Bob. Meanwhile, the index and data BER performance at Eve remain at 0.5, showing the remarkable secrecy performance gain achieved by S-FAIM. Since the wavelet scattering network operates efficiently with small training datasets, S-FAIM can adapt to various attack scenarios by adjusting the training datasets.

V. Conclusion

In this paper, we have designed a novel secure fluid antenna index modulation (S-FAIM) framework with SEFDM waveforms. CSI-based mapping rule between index bits and channel conditions, achieved through adjustments in fluid antenna port positions, is proposed for confidential index transmission. Meanwhile, secure data symbol transmission is realized by exploiting non-orthogonal waveforms and LDPC coding. Simulation results verify that the proposed S-FAIM system enables additional index transmission without degrading data symbol transmission at the legitimate receiver, while ensuring constant error floors at 0.5 for the eavesdropper.

VI. Acknowledgement

This work was supported by the UK Engineering and Physical Sciences Research Council (EPSRC) under Grant EP/Y000315/1.

References

[1] Y. Wu, A. Khisti, C. Xiao, G. Caire, K.-K. Wong, and X. Gao, "A survey of physical layer security techniques for 5G wireless networks and challenges ahead," *IEEE Journal on Selected Areas in Communications*, vol. 36, no. 4, pp. 679–695, 2018.

[2] U. Maurer, "Secret key agreement by public discussion from common information," *IEEE Transactions on Information Theory*, vol. 39, no. 3, pp. 733–742, 1993.

[3] J. Zhang, A. Marshall, R. Woods, and T. Q. Duong, "Design of an OFDM physical layer encryption scheme," *IEEE Transactions on Vehicular Technology*, vol. 66, no. 3, pp. 2114–2127, 2017.

[4] T. Mao, Q. Wang, Z. Wang, and S. Chen, "Novel index modulation techniques: A survey," *IEEE Communications Surveys Tutorials*, vol. 21, no. 1, pp. 315–348, 2019.

[5] S. Sugiura, T. Ishihara, and M. Nakao, "State-of-the-art design of index modulation in the space, time, and frequency domains: Benefits and fundamental limitations," *IEEE Access*, vol. 5, pp. 21 774–21 790, 2017.

[6] R. Y. Mesleh, H. Haas, S. Sinanovic, C. W. Ahn, and S. Yun, "Spatial modulation," *IEEE Transactions on Vehicular Technology*, vol. 57, no. 4, pp. 2228–2241, 2008.

[7] A. K. Khandani, "Media-based modulation: A new approach to wireless transmission," in *2013 IEEE International Symposium on Information Theory*, 2013, pp. 3050–3054.

[8] E. Basar, "Media-based modulation for future wireless systems: A tutorial," *IEEE Wireless Communications*, vol. 26, no. 5, pp. 160–166, 2019.

[9] E. Faddoul, Y. Guo, G. M. Kraidy, C. Psomas, and I. Krikidis, "Correlation mitigation schemes for index-modulated fluid antenna systems," in *GLOBECOM 2023 - 2023 IEEE Global Communications Conference*, 2023, pp. 5324–5329.

[10] J. Zhu, G. Chen, P. Gao, P. Xiao, Z. Lin, and A. Quddus, "Index modulation for fluid antenna-assisted MIMO communications: System design and performance analysis," *IEEE Transactions on Wireless Communications*, pp. 1–1, 2024.

[11] Y. Chen and T. Xu, "Fluid antenna index modulation communications," *IEEE Wireless Communications Letters*, vol. 13, no. 4, pp. 1203–1207, 2024.

[12] Y. Chen, T. Xu, and I. Darwazeh, "Index modulation pattern design for non-orthogonal multicarrier signal waveforms," *IEEE Transactions on Wireless Communications*, vol. 21, no. 10, pp. 8507–8521, 2022.

[13] K.-K. Wong, A. Shojaeifard, K.-F. Tong, and Y. Zhang, "Fluid antenna systems," *IEEE Transactions on Wireless Communications*, vol. 20, no. 3, pp. 1950–1962, 2021.

[14] S. Mallat, *A Wavelet Tour of Signal Processing, Third Edition: The Sparse Way*, 3rd ed. Orlando, FL, USA: Academic Press, Inc., 2008.

[15] J. Andén and S. Mallat, "Deep scattering spectrum," *IEEE Transactions on Signal Processing*, vol. 62, no. 16, pp. 4114–4128, Aug. 2014.

[16] Y. Chen, W. Yuan, and T. Xu, "Coding split and adjustment to defend OFDM-IM against jamming attacks," *IEEE Communications Letters*, vol. 27, no. 2, pp. 457–461, 2023.

[17] Y. Chen, C. Wang, J. Si, and T. Xu, "Anti-eavesdropping and anti-jamming waveform design with coding split index modulation," in *2023 IEEE/CIC International Conference on Communications in China (ICCC)*, 2023, pp. 1–6.